10954 *Inorg. Chem.* **2009**, *48*, 10954–10971
DOI: 10.1021/ic900995u

Inorganic Chemistry
Article

Oxalate Bridged MM (MM = Mo_2, MoW, and W_2) Quadruply Bonded Complexes As Test Beds for Current Mixed Valence Theory: Looking beyond the Intervalence Charge Transfer Transition†

Benjamin J. Lear and Malcolm H. Chisholm*

Department of Chemistry, The Ohio State University, Columbus, Ohio 43210

Received May 21, 2009

The spectroscopic features of a series of oxalate bridged complexes $[(^tBuCO_2)_3MM]_2$-μ_2-O_2CCO_2 (where MM = Mo_2, MoW, and W_2) in their neutral and singly oxidized (mixed valence) states are examined as a function of temperature and solvent. A large degree of electronic coupling between the two MM centers is evident, principally involving the MM δ orbitals mediated by the oxalate bridge π^* orbital. In the oxidized states these mixed valence ions show solvent independent intervalence charge transfer (alternatively termed charge resonance) bands, consistent with assignment to Class III (or electronically delocalized) within the Robin−Day classification scheme. In both the neutral and oxidized states these complexes also show an intense metal-to-ligand charge-transfer (MLCT) transition, involving the lowest unoccupied molecular orbital (LUMO) of the bridge. The solvent and temperature dependence of this transition is also reported along with an inspection and simulation of the vibronic features, which are notably altered when switching between the neutral and the mixed valence states as well as with variation of the nature of the MM unit. Collectively, these observations allow us to comment on the validity and limitations of current theories dealing with mixed valence ions that have hitherto ignored the information that can be gained from MLCT transitions.

Introduction

Over the past four decades, beginning with the Creutz-Taube (C-T) ion, the purposeful synthesis of mixed valence complexes has allowed for the systematic study of intramolecular electron transfer and the parameters that govern this event. In the course of this research Marcus−Hush theory[1,2] has emerged as the dominant theory, as it provides a simple intuitive picture that can explain many of the properties exhibited by these systems. This theory treats the transfer of an electron between two redox centers as the transfer between two electronic states that are allowed to electronically couple. Since its introduction, it has been modified to explicitly include various additional properties such as vibronic coupling,[3] additional important electronic states[4] (such as electronic occupation of the bridge), and tunneling.[5]

Of these modifications, the one that is of the greatest importance to the interpretation of the study reported herein is the three-state model as first proposed by Ondrechen and co-workers.[4] This is a model that accounts for explicit electronic occupation of the bridging ligand in a mixed valence compound. Thus, the model starts with three diabatic states, two of which are accounted for by electronic occupation of the two redox centers between which the electron exchanges, while the third state is defined by electronic occupation of the bridge (Figure 1a). These three states are (assuming the harmonic oscillator approximation) drawn as parabolas in a coordinate system composed of three axes accounting for asymmetric nuclear motion, symmetric nuclear motion, and the energy of the system. The two states associated with electronic occupation of the redox sites (red and blue) are offset from one another along the asymmetric coordinate (sometimes referred to as the reaction coordinate), as movement of an electron from one redox site to the other will result in the bonds in the coordination sphere of one site lengthening while, at the other site, the corresponding bonds contract. Thus, the overall change in geometry accompanying the movement of an electron is one of an asymmetric stretch. Following similar reasoning, the state arising from electronic occupation of the bridge (green) is drawn intermediate to the two redox-based states along the asymmetric coordinate (transfer of the unpaired electron to the bridge gives a state in which both sites are oxidized) and offset along the symmetric coordinate (transfer of the unpaired electron to the bridge affects the bridge bonds symmetrically, having

† Dedicated to Peter Day on the occasion of his 70th birthday.

*To whom correspondence should be addressed. E-mail: chisholm@chemistry.ohio-state.edu.

(1) Marcus, R. A. *J. Chem. Phys.* **1956**, *24*, 966–978.
(2) Hush, N. S. *Prog. Inorg. Chem.* **1967**, *8*, 391–444.
(3) Piepho, S. B.; Krausz, E. R.; Schatz, P. N. *J. Am. Chem. Soc.* **1978**, *100*, 2996–3005.
(4) Ondrechen, M. J.; Ko, J.; Zhang, L. T. *J. Am. Chem. Soc.* **1987**, *109*, 1672–1676.
(5) Gray, H. B.; Winkler, J. R. *Proc. Natl. Acad. Sci. U.S.A.* **2005**, *102*, 3534–3539.

 Published on Web 10/27/2009 © 2009 American Chemical Society

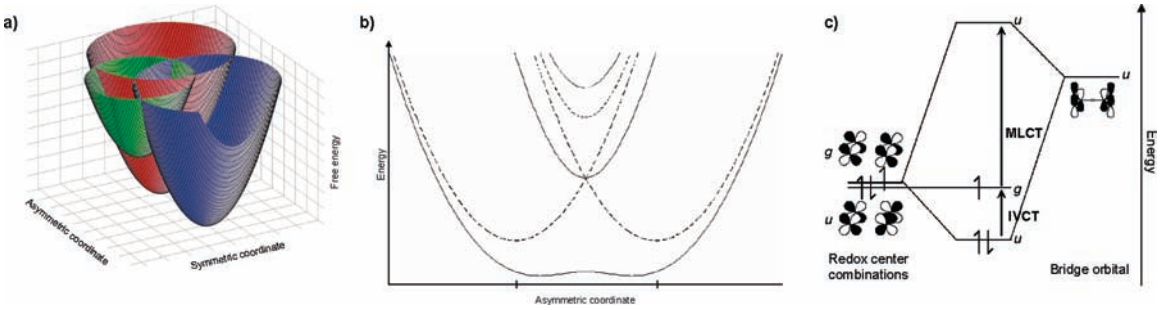

Figure 1. (a) PES associated with the diabatic states employed in the three state model. They are composed of two redox-based states (red and blue) and a bridge-based state (green). (b) Cross-section along the asymmetric coordinate that shows the original diabatic states (dashed lines) and the new adiabatic states (solid lines) that result from electronic coupling between the diabatic states. (c) MO diagram depicting the coupling between the bridge and metal−metal combinations of **1**−**3** commonly invoked in discussion of delocalized complexes under the three state model. The bonding and antibonding type orbitals result from coupling between the bridge LUMO and the in-phase combination of the two MM δ bonds. The non-bonding orbital is composed of the out-of-phase combination of the two MM δ bonds.

Scheme 1. Complexes **1**, **2**, and **3**, Which Form a Series of Oxalate Bridged Dimers That Differ Only in the Relative Ratio of Tungsten to Molybdenum

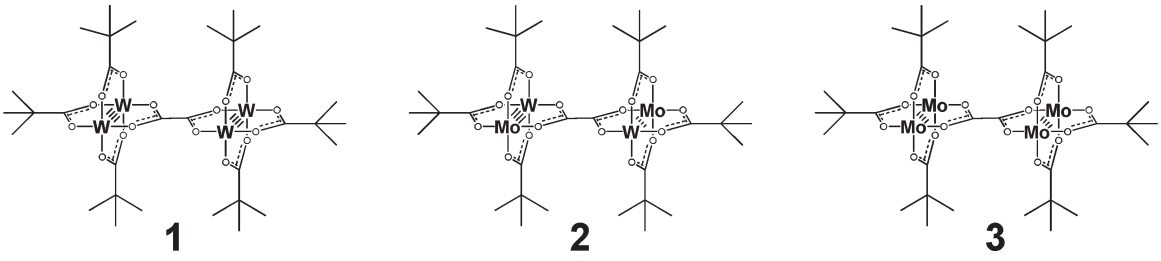

the symmetry of a symmetric stretch). In the case shown in Figure 1, the bridge-based state is also depicted as higher in energy than the two redox-based states, consistent with the fact that electronic occupation of the bridge is an excited state. These three diabatic states may couple to one another to give three new, adiabatic, states. Figure 1b shows a cross section of these new states along the asymmetric (reaction) coordinate.

In the case that electronic coupling is strong enough to give rise to an electronically delocalized ground state, it has been common to discuss these three new states by employing a molecular orbital (MO) picture (as shown in Figure 1c) to aid in visualizing the coupling in the system. Here we consider the redox units and bridge for the complexes used in the study we are reporting (Scheme 1). In the MO picture we consider two combinations (in-phase and out-of-phase) of the MM δ orbitals and how they interact with the oxalate lowest unoccupied MO (LUMO). Thus, one MO is stabilized by a bonding interaction between the in-phase δ combination and the bridge, while one is destabilized by an antibonding interaction between the bridge and the in-phase δ combination. The third MO is composed of the out-of-phase δ combination, which is not of proper symmetry to interact with the bridge. As such, the energy of this third MO remains unaffected by coupling to the bridge. By symmetry, there are two allowed electronic transitions in this diagram: (i) the highest occupied MO (HOMO) to the singly occupied MO (SOMO) transition (containing some ligand to metal charge transfer character), which is commonly called the intervalence charge transfer (IVCT) transition, and (ii) the SOMO to LUMO transition (largely metal to ligand charge transfer in nature) which is called the metal-to-ligand charge-transfer (MLCT) transition. While it is common to use the state and orbital pictures interchangeably, it is important to realize that these two descriptions are fundamentally different. The orbital picture provides us with an understandable image of where electrons reside, whereas the *states* that actually electronically couple in mixed valence systems are defined by the electronic occupancy of these orbitals. In particular, it is important to realize that the coupling between *states* (shown in Figure 1a and b) is **not** the same as coupling between orbitals (as depicted in Figure 1c). This is one of the major themes of this paper and will be revisited in greater detail in the course of the discussion.

The advantage of this three state model is 3-fold. First, it acknowledges the importance of the bridge, which can effect the degree of coupling in a mixed valence complex through changes to the symmetry of the bridge as well as the energy gap between the redox sites and bridge orbital. Second (and perhaps more importantly), the MLCT and IVCT bands are both explicitly affected by the coupling between the redox and bridge based states. This enables one to explain changes to both the IVCT and MLCT bands that result from the electronic coupling in the mixed valence oxidation state. Lastly, inclusion of the bridge allows for an understanding of how bridge vibrational modes may be coupled to electronic transitions. In Figure 1a the bridge-based state is offset from the metal based states along a symmetric coordinate associated, in part, with a symmetric stretch of the bridge. This necessarily results in vibronic coupling of the MLCT and IVCT transitions to symmetric modes of the bridge. Indeed, it has been shown that IVCT transitions in mixed valence complexes, such as the C-T ion, can best be reproduced by incorporating vibronic coupling involving bridge vibrations.[4]

The ability to reproduce the IVCT band of the C-T ion was an important milestone in the field of mixed valence research. The C-T complex appears to belong to a recently recognized class of mixed valence complexes, Class II−III,[6] which span

(6) Demadis, K. D.; Hartshorn, C. M.; Meyer, T. *J. Chem. Rev.* **2001**, *101*, 2655–2685.

the transition from a strongly coupled, but localized ground electronic state to one that is delocalized (Class II and Class III, respectively, in the Robin−Day mixed valence classification scheme[7]). The three state model (with its associated vibronic coupling to symmetric bridge-based modes) allows for the understanding of the observance of strong vibronic coupling in Class II−III and Class III complexes, whereas in the two state model the potential energy surfaces (PES) would be nested along the sole (reaction) coordinate, predicting minimal vibronic coupling.

From consideration of the three state model it is clear that the shape of the IVCT transition contains a significant degree of information concerning the shape of the ground state PES as well as the relative orientation of the ground and excited state PES along the symmetric coordinate. Interestingly, despite the fact that under this model the MLCT band should also contain similar information, there presently appears to be no experimental study that deals explicitly with the MLCT transition in mixed valence complexes and how the properties of this transition are affected by electronic coupling. Here, we examine both the IVCT and MLCT transitions of three related complexes (**1**, **2**, and **3** in Scheme 1) in their neutral and mixed valence (+1) oxidation states.

The spectral features of this series of complexes (all three previously assigned to class III[8−10]) are much simpler than those of the related mononuclear d^5-d^6 mixed valence systems that are complicated by d-d electronic configuration interactions, spin−orbit coupling, and low symmetry elements about the metal ions, giving rise to spectra in which the IVCT band often cannot be unequivocally established. Also, within this series of MM linked complexes, we have the unique opportunity of examining the stepwise change of metal within the MM units: MM = Mo_2, MoW, and W_2. For these reasons the spectroscopic features of the complexes discussed herein warrant the detailed attention of the present study with respect to current theories of mixed valence ions. Some of the spectral features of these complexes and their mixed valence ions have been described previously, but not within the context of and aim toward extending the current theories of electronic coupling and mixed valency. In this regard, the studies and analysis reported herein challenge and advance the interpretation of the coupling and spectroscopic properties of mixed valence complexes.

In this paper, the IVCT transition is used to frame the discussion with respect to the established literature of mixed valence chemistry. We then pay particular attention to changes to the MLCT transition that accompany generation of the mixed valence ion. Specifically, we examine the vibronic coupling as well as the solvent and temperature dependence of the MLCT of **1**−**3**. We use this information to discuss the ground state electronic structure of these complexes as well as the relationship between the ground and excited state PES. We conclude by suggesting further experiments that will help to elucidate the connection between the properties of electronic transitions and electronic structure of mixed valence systems.

Experimental Methods

Chemicals. Compounds **1**−**3** were prepared using published procedures.[11] $AgPF_6$ was obtained from Aldrich and used without further purification. Solvents were obtained from Fisher and dried using standard techniques. All manipulations were carried out under a purified N_2 atmosphere using standard procedures for the manipulation of air-sensitive materials. All mixed valence ions were generated chemically by stoichiometric addition of $AgPF_6$ to a solution of **1**, **2**, or **3**. For **1** and **2**, based upon analysis of the MLCT band, the cations are generated with ∼100% yield. For **3**, the best yield we were able to observe, based upon analysis of the MLCT band, was about 60%. For or all three mixed valence cations, their generation was followed by redox disproportionation, though the rate of disproportionation varies by complex, being faster with increasing molybdenum content in the MM unit.

Spectroscopy. Room temperature UV−vis and NIR spectra were obtained using a Perkin-Elmer Lambda 900 UV−vis NIR spectrometer and a 1 mm path length NIR quartz cell. Low temperature spectra were obtained using the same spectrometer and a Specac variable temperature cryostat employing a permanently sealed liquid IR cell with CaF_2 windows. The use of CaF_2 proved to be critical, as the mixed valence species were not persistent in cells employing KBr windows. Integrated intensities of electronic absorption bands were obtained using Microcal Origin 6.0. The Raman spectrum for **2** was obtained using a *Renishaw inVia* Raman spectrometer using 785 nm laser excitation. Resonance Raman spectra for **1** and **3** were previously reported.[8]

Simulation of the MLCT and IVCT Bandshapes. The simulation MLCT and IVCT bandshapes for **1**−**3** in the neutral and mixed valence state was performed using *Ramint*, a program written in Fortran by Professor Anne Kelley, which employs a time dependent approach to electronic spectra, as developed by Heller.[12,13] Detailed accounts of these types of calculations can be found elsewhere;[14−18] however, we very briefly touch upon the underlying concepts here.

This approach for the calculation of electronic absorption spectra finds its basis in the following equation.[19]

$$I(\omega) \propto \omega \int_{-\infty}^{\infty} e^{i\omega t}\langle\phi|\phi(t)\rangle \, dt \qquad (1)$$

which gives the intensity of an absorption feature at a particular frequency. The aspect of this approach that we will be most interested in is the dependence of absorption features upon the autocorrelation function, $\langle\phi|\phi(t)\rangle$, which examines the overlap of the dynamically evolving excited state *wavepacket* with the static ground state *wave function*. [This is depicted in Figure 14b and addressed in detail elsewhere.] One critical result of this dependence is that the features of absorption bands are determined, in part, by the evolution of the system *after* the excitation. This, in turn, is related to the slope of the PES that is initially populated and, thus, allows one to gain insight into the

(7) Robin, M. B.; Day, P. *Adv. Inorg. Chem. Radiochem.* **1967**, *10*, 247–422.
(8) Bursten, B. E.; Chisholm, M. H.; Clark, R. J. H.; Firth, S.; Hadad, C. M.; MacIntosh, A. M.; Wilson, P. J.; Woodward, P. M.; Zaleski, J. M. *J. Am. Chem. Soc.* **2002**, *124*, 3050–3063.
(9) Chisholm, M. H.; Patmore, N. J. *Acc. Chem. Res.* **2007**, *40*, 19–27.
(10) Cayton, R. H.; Chisholm, M. H. *J. Am. Chem. Soc.* **1989**, *111*, 8921–8923.
(11) Cayton, R. H.; Chisholm, M. H.; Huffman, J. C.; Lobkovsky, E. B. *J. Am. Chem. Soc.* **1991**, *113*, 8709–8724.
(12) Heller, E. J. *Acc. Chem. Res.* **1981**, *14*, 368–375.
(13) Lee, S.; Heller, E. J. *J. Chem. Phys.* **1979**, *71*, 4777–4788.
(14) Doorn, S. K.; Hupp, J. T. *J. Am. Chem. Soc.* **1989**, *111*, 4704–4712.
(15) Doorn, S. K.; Hupp, J. T.; Porterfield, D. R.; Campion, A.; Chase, D. B. *J. Am. Chem. Soc.* **1990**, *112*, 4999–5002.
(16) Hupp, J. T.; Williams, R. D. *Acc. Chem. Res.* **2001**, *34*, 808–817.
(17) Myers, A. B. *Chem. Rev.* **1996**, *96*, 911–926.
(18) Myers, A. B. *Acc. Chem. Res.* **1997**, *30*, 519–527.
(19) Tutt, L. W.; Zink, J. I.; Heller, E. J. *Inorg. Chem.* **1987**, *26*, 2158–2160.

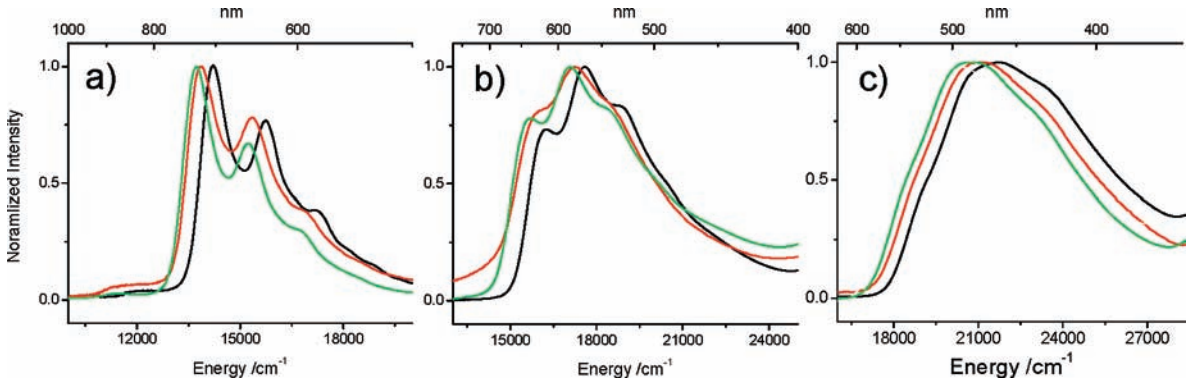

Figure 2. MLCT band for (a) **1**, (b), **2**, and (c) **3** in THF (black line), CH_3CN (red line), and DMF (green line) at 298 K.

offsets of the PES along coordinates associated with specific nuclear adjustments (vibrational modes).

The program that we use to simulate the electronic absorption profiles gives the user the ability to vary 11 parameters. These include the number of Raman active modes, the inhomogeneous broadening, the frequency assigned to collective modes of the solvent, the temperature, the E_{0-0}, the homogeneous broadening, the Brownian oscillator line shape parameter, the length of the charge transfer accompanying the electronic excitation, the solvent refractive index, the frequency of each Raman mode, and the dimensionless offsets of the minima of the initial and final PES along a coordinate associated with each Raman active frequency. Of these 11 parameters, two (temperature and solvent refractive index) are defined by the conditions of the experiment, three (number of Raman active modes, their frequency, and E_{0-0}) can be determined experimentally, and two (Brownian oscillatory line shape and collective modes of the solvent) have standard values. The length of charge transfer for the IVCT and MLCT transitions can be estimated from crystallographic data[8,20] and was taken to be 7 Å for the IVCT and 3.5 Å for the MLCT for all the complexes in this study. This leaves the inhomogeneous broadening, homogeneous broadening, and the dimensionless offsets for each Raman mode as the adjustable parameters. For each complex the dimensionless offsets were changed with changes in oxidation state, and the broadening parameters were changed for each state with changes in temperature. Because for each complex at two temperatures we only vary the dimensionless offsets along the coordinates associated with each Raman mode, this provides us a way to determine the offsets of the PES along the nuclear coordinates associated with these modes and to monitor how they change upon generation of the mixed valence state.

Results

Solvent and Temperature Dependence of the MLCT of the Neutral Complexes. The MLCT bands for **1**−**3** in tetrahydrofuran (THF), CH_3CN, and *N*,*N*-dimethylformamide (DMF) at 298 K are shown in Figure 2. For each complex, the MLCT transition can be assigned as a δ to π^* transition, in which the π^* orbital lies almost entirely on the bridging oxalate (the LUMO of the bridge).[8] Some of these spectra have been reported previously;[8,9,11] however, they are presented here to aid in discussion of the properties of the MLCT bands for **1**−**3** and how they are affected by changes in solvent, temperature, and oxidation state of the complex. There are three aspects to note concerning these spectra. First, each MLCT band displays marked vibronic features, though the degree to which these features are resolved varies between the complexes, with resolution increasing with tungsten content. Second, the energy of this transition also varies between complexes, with the energy decreasing with increasing tungsten content reflecting the fact that the tungsten δ orbitals lie higher in energy than do the δ orbitals of molybdenum (decreasing the energy gap between the δ orbital and the LUMO of the bridge). Third, each complex shows strong solvatochromism. The position of the lowest energy vibronic feature in each solvent can be found in Table 1, which summarizes the room temperature solvent dependence of the charge transfer (MLCT and IVCT) transitions for **1**−**3** in both their neutral and their mixed valence states. Table 2 summarizes information concerning the shape and intensity of these bands in THF. The solvent dependence shows a trend of increasing energy with decreasing solvent polarity. In addition, the magnitude of the solvatochromism follows the trend **3** > **2** > **1**.

Table 1. Position of the First Vibronie Feature for the MLCT and IVCT at 298 K in THF, CH_3CN, and THF of the Neutral and Mixed Valence States of **1**, **2**, and **3**

Neutral State			
compound	THF cm^{-1}	CH_3CN cm^{-1}	DMF cm^{-1}
	MLCT		
1	14210	13870	13740
2	16230	16100	15720
3	19380	18960	18610
Mixed Valence State			
compound	THF cm^{-1}	CH_3CN cm^{-1}	DMF cm^{-1}
	MLCT		
$\mathbf{1}^+$	15040	15060	14970
$\mathbf{2}^+$	14030	14080	
$\mathbf{3}^+$	15650		
	IVCT		
$\mathbf{1}^+$	5988	5974	5963
$\mathbf{2}^+$	5076	5084	5115
$\mathbf{3}^+$	1560		

The vibronic features observed within the MLCT band in these complexes can be sharpened by lowering the temperature of the system, and Figure 3 shows the MLCT bands for **1**−**3** in 2-MeTHF at both 298 and 100 K.

(20) Cotton, F. A.; Donahue, J. P.; Lin, C.; Murillo, C. A. *Inorg. Chem.* **2001**, *40*, 1234–1244.

Table 2. Position, Width, And Extinction Coefficient for the MLCT and IVCT of the Neutral and Mixed Valence States of **1**, **2**, and **3** in THF at 298 K

Neutral State					
compound	ν_{max}	fwhm cm^{-1}	width (1/e) cm^{-1}	ε (ν_{max})	ε (integrated)
MLCT					
1	14230	2494	3653	36400	106.0
2	17610	4739	4679	21060	102.3
3	21790	6867	8728	14200	91.43

Mixed Valence State					
compound	ν_{max} cm^{-1}	fwhm cm^{-1}	width (1/e) cm^{-1}	ε (ν_{max}) M^{-1} cm^{-1}	ε (integrated) M^{-1} $cm^{-2}(10^6)$
MLCT					
$\mathbf{1}^+$	15040	1350	1750	42560	78.21
$\mathbf{2}^+$	15650	2140	3020	24390	104.90
$\mathbf{3}^+$	15650	1280	2050	16171	32.49[a]
IVCT					
$\mathbf{1}^+$	5988	839	1058	5620	5.69
$\mathbf{2}^+$	5076	1214	1522	9546	12.90
$\mathbf{3}^+$	4085	1848[b]	2333[b]	6000	5.88

[a] $\mathbf{3}^+$ rapidly disproportionates to regenerate the neutral species. Additionally, the MLCT band of the mixed valence and neutral states overlap. As such, this value for the integrated intensity of the MLCT for the mixed valence state is a lower limit. [b] The IVCT band for $\mathbf{3}^+$ is highly asymmetric. The values reported here are for the observed band, rather than for the extrapolated pure Gaussian shape.

Again, there are several things to note about these spectra. First, reduction in temperature is accompanied by a shift in the location of the band to lower energy. Also of note in these spectra is that the underlying vibronic features are much better resolved at low temperature (though the degree of resolution still increases with relative tungsten content). Indeed, for all three complexes at low temperature two distinct vibronic progressions are observable. The spacing of these vibronic features can be obtained from Table 3, which summarizes the features of the low temperature spectra for both the neutral and mixed valence states of **1**−**3**. Also of note, concerning the vibronic features, is the relative intensity of the features within each progression. For **1** the first vibronic feature is the most intense while for **2** and **3** it is the second feature that is the most intense in the progression (this feature having the most relative intensity for **3**). The resulting general trend is one of increasing relative intensity of the second feature with increasing molybdenum content.

We find that the low temperature solvent dependence of the MLCT band is significantly reduced from that observed for the room temperature spectra. Figure 4 shows the MLCT bands of **1**−**3** in 2-MeTHF and DMF at 100 K, and the energies of the first vibronic feature are recorded in Table 3. DMF does not form a glass when frozen and so the spectra reported for DMF are the result of averaging six individual spectra and then smoothing the resulting spectrum over 5 adjacent points. While the final spectrum obtained in this manner remains quite noisy, the maximum of the vibronic features of interest are clearly identifiable. As a result, we find the solvent dependence at low temperature for **1**−**3** is reduced by at least 50%, when compared to the room temperature dependence. Lastly, it should be pointed out that the solvatochromism is reversed in the low temperature spectra. That is, the transitions are at higher energy in DMF than in 2-MeTHF (they were at lower energy in DMF versus THF at room temperature).

Solvent and Temperature Dependence of the Mixed Valence Dimers' IVCT Transition. Figure 5 displays the room temperature IVCT band for $\mathbf{1}^+$ and $\mathbf{2}^+$ in THF, CH_3CN, and DMF and for $\mathbf{3}^+$ in THF. Table 1 summarizes the solvent dependence of and Table 2 contains information on the shape and intensity of these bands. The solvent dependence of the IVCT band for $\mathbf{3}^+$ could not be investigated because of limited solubility of the mixed valence ion in solvents other than THF. There are two properties of note in these spectra. First, the IVCT band for both $\mathbf{1}^+$ and $\mathbf{2}^+$ displays very little solvatochromism. Second, these bandshapes lack resolved vibronic structure and appear to be relatively symmetric. Indeed, for both $\mathbf{1}^+$ and $\mathbf{2}^+$ the IVCT band and its mirror image are virtually superimposable upon one another (see Supporting Information). However, it should be noted that the IVCT band for $\mathbf{2}^+$ is clearly more asymmetric than for $\mathbf{1}^+$. Thus, we find that the symmetry of the IVCT band increases with increasing tungsten content (or, as we will see, the degree of electronic coupling).

The IVCT band of $\mathbf{1}^+$−$\mathbf{3}^+$ was also recorded at low temperature (100 K) in 2-MeTHF glasses in the hopes that any underlying vibronic features present could be better resolved. Figure 6 compares the IVCT bands for $\mathbf{1}^+$ and $\mathbf{2}^+$ at 100 and 298 K in 2-MeTHF. Because of the kinetic lability of $\mathbf{3}^+$, the low temperature spectrum for this ion could not be obtained. For $\mathbf{1}^+$ a single low intensity feature is present with a spacing of ~600 cm^{-1}, an energy that corresponds well with the ν_3 mode of the oxalate. No other features are observed in the IVCT band of $\mathbf{1}^+$. For $\mathbf{2}^+$ no distinct features appear for the IVCT band at low temperature, though the asymmetric shape of this band becomes accentuated. As the IVCT band showed no solvent dependence at room temperature, the low temperature solvent dependence was not investigated.

Solvent and Temperature Dependence of the MLCT Transition for the Mixed Valence Dimers. The MLCT band for **1**−**3** undergoes significant changes upon oxidation to the mixed valence state. Figure 7 compares the MLCT band in THF of $\mathbf{1}^+$ with **1**, $\mathbf{2}^+$ with **2**, and $\mathbf{3}^+$ with **3**. Table 1 summarizes the position of the first vibronic feature for the mixed valence ions. The most striking change to the MLCT band is the reduction in the vibronic features upon generation of the mixed valence cation. This is most pronounced for $\mathbf{1}^+$, in which the vibronic structure appears to be completely lost and only a single somewhat symmetric band remains, but the loss of vibronic coupling is displayed by all three complexes. The MLCT band for $\mathbf{1}^+$ is quite clean and appears to be uncluttered by other electronic transitions. The MLCT for $\mathbf{2}^+$ has a feature on the low energy side that at first glance might be taken for a vibronic feature. However, the fact that the overall shape of the band cannot be adequately simulated treating this as a vibronic feature (*vide infra*) as well as the fact that the position of this

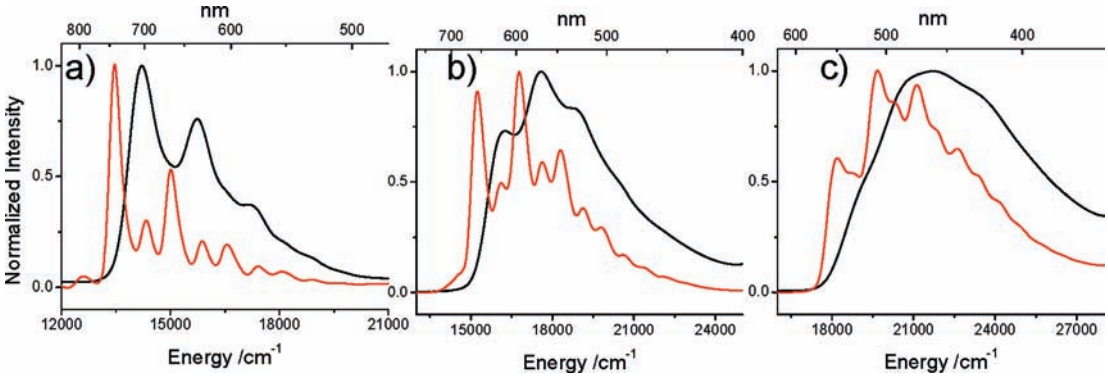

Figure 3. MLCT band for (a) **1**, (b), **2**, and (c) **3** in 2-MeTHF at 298 K (black) and 100 K (red).

Table 3. Positions of the Vibronic Features Observed for the MLCT Transition for the Neutral and Mixed Valence States of **1**, **2**, and **3** at 100 K in 2-MeTHF and DMF[a]

Neutral State					
MLCT					
1		**2**		**3**	
2-MeTHF cm^{-1}	DMF cm^{-1}	2-MeTHF cm^{-1}	DMF cm^{-1}	2-MeTHF cm^{-1}	DMF cm^{-1}
13459	**13643**	15244	15649	18200	18450
14327	14514	16129	**17050**	18762	20534
15015	15291	**16779**	17762	**19685**	21367
15873	16155	17637	18519	20243	**21978**
16556	16807	18315	19646	21120	
17422	17762	19120	20121	21786	
18083	18349	18902	21097	22624	
18904	19194	20619		23364	
19685		21322		24096	
20491		22124		24876	
		22883			
Mixed Valence State					
MLCT					
1+		**2+**		**3+**	
2-MeTHF cm^{-1}		2-MeTHF cm^{-1}		2-MeTHF cm^{-1}	
14859		13928		n/a	
15385		**15361**			
16340		17889			
		19380			
		20833			
		22573			
		23810			

[a] The position of the most intense feature is in bold.

feature does not change with changes in temperature (as does the main feature) leads us to believe that it has another origin. Complexes of this type are known to form aggregates in some solvents which give rise to a lower energy MLCT transition than for those still in solution.[21] It seems likely to us that this low energy feature arises from an aggregation of the charged 2^+ species. The MLCT band for 3^+ is somewhat complicated by the fact that it overlaps strongly with the MLCT for **3**, which is present in significant quantities as 3^+ undergoes relatively rapid redox disproportionation. It is worth noting that there appears to be a vibronic progression in the MLCT band for 3^+, but that its entire length is obscured by this overlap with the MLCT band from **3**. It is also worth mentioning that in the mixed valence states of **1**−**3** the extinction coefficient at the maximum of the MLCT band is much larger than for the neutral species and the *integrated* intensity (related to the oscillator strength for the transition) remains significant (Table 2).

The room temperature solvent dependence of the MLCT transition in the mixed valence ions can be seen in Figure 8, where the MLCT bands for 1^+ and 2^+ in THF, CH_3CN, and DMF at room temperature are displayed. The energy of the first vibronic feature can be found in Table 1. Again, as for the IVCT transition, the solvent dependence of the MLCT transition for 3^+ could not be obtained because of insolubility in solvents other than THF. The solvent dependence of this transition for 1^+ and 2^+ is reduced as compared to the MLCT transition for the neutral complexes. The smallest solvatochromism is displayed by 1^+, in which the solvent dependence is only 15% of that found in the neutral state.

Just as for the neutral complexes, the vibronic structure in the MLCT bands for 1^+ and 2^+ can be better resolved at low temperature. Figure 9 shows the MLCT band for 1^+ and 2^+ in 2-MeTHF at 298 and 100 K. The low temperature features are summarized in Table 2. Because of rapid disproportionation of 3^+ that regenerates **3**, the temperature dependence of 3^+ could not be obtained. Of note is that the MLCT band for 1^+, which appeared to be featureless at room temperature, is revealed to be composed of three vibronic features (belonging to two different vibronic progressions). In the mixed valence state, the relative intensity of the lowest energy feature has increased significantly, and the second and third features are very weak. Interestingly, the MLCT band of 2^+ displays very little change upon reduction of the temperature and, as such, no new vibronic features are identified at low temperature. However, redox disproportionation of 2^+ occurs sufficiently rapidly that a nontrivial amount of **2** is present in solution by the time that the cryostat reaches 100 K and features associated with **2** can be seen on the high energy side of the MLCT band. Perhaps the presence of **2** obscures whatever vibronic features may be present in the MLCT band for 2^+. Also of note is that the MLCT transitions for the mixed valence complexes show reduced temperature dependence as compared to

(21) Chisholm, M. H.; Patmore, N. J. *Inorg. Chem. Acta* **2004**, *357*, 3877–3882.

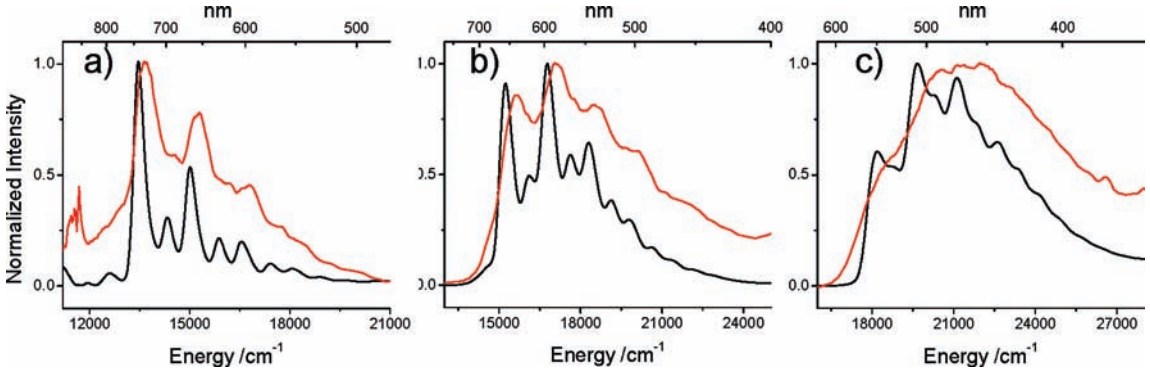

Figure 4. MLCT band for (a) **1**, (b), **2**, and (c) **3** in 2-MeTHF (black line) and DMF (red line) at 100 K.

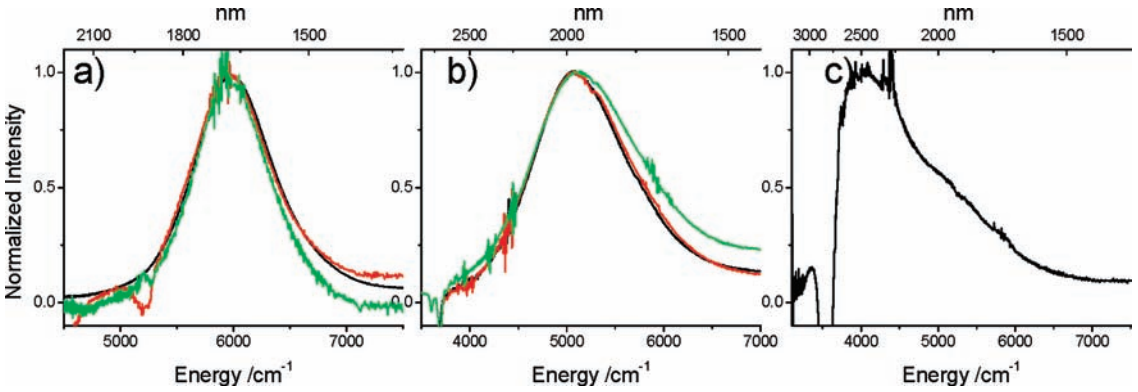

Figure 5. IVCT bands for (a) $\mathbf{1}^+$ and (b) $\mathbf{2}^+$ in THF (black line), CH_2Cl_2 (green line), and CH_3CN (red line) at room temperature as well as (c) $\mathbf{3}^+$ in THF.

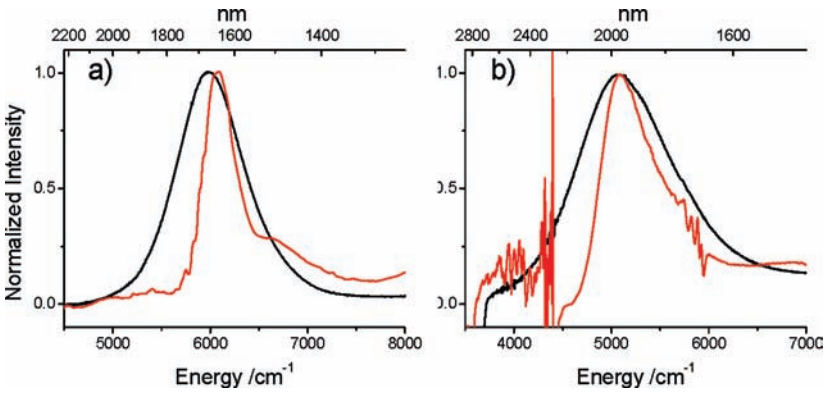

Figure 6. IVCT band for (a) $\mathbf{1}^+$ and (b) $\mathbf{2}^+$ in 2-MeTHF at 298 K (black line) and 100 K (red line).

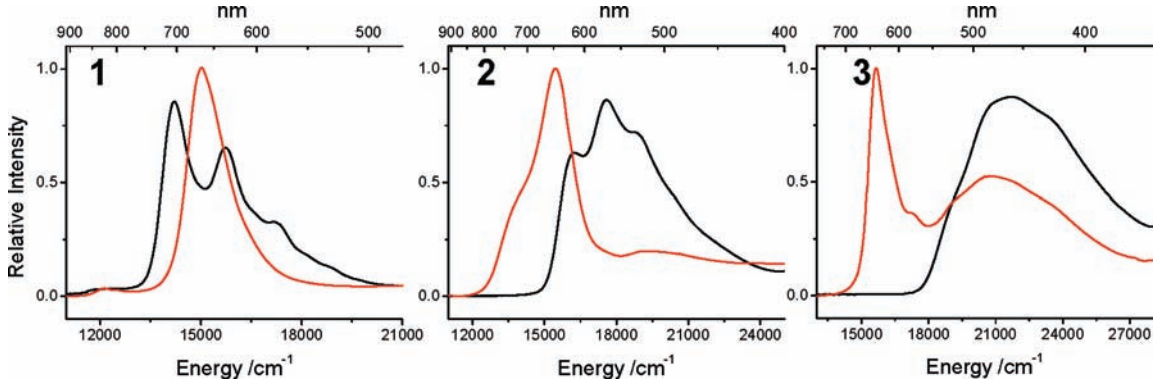

Figure 7. Comparison of the MLCT bands for the neutral (black) and mixed valence (red) states in THF for **1**−**3**.

the MLCT transitions of the neutral species. As was the case for the change in solvent dependence and the change in the vibronic structure, this change is most dramatic in the case of $\mathbf{1}^+$.

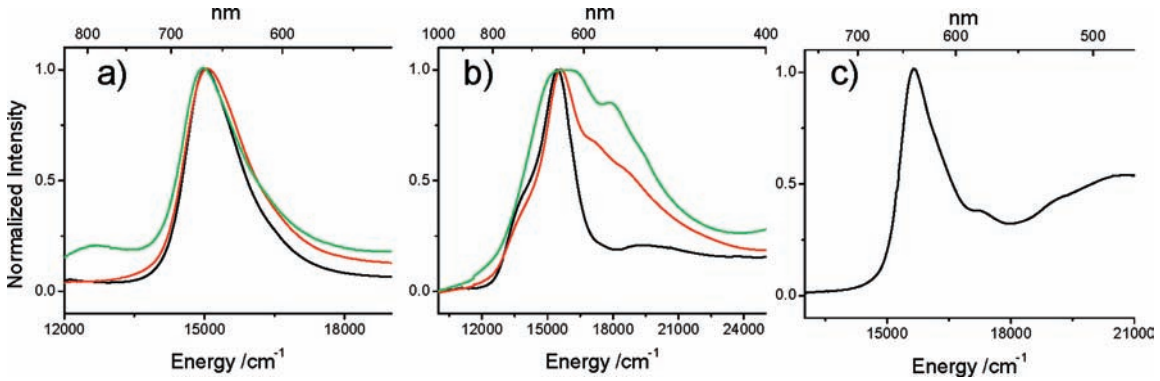

Figure 8. MLCT bands for (a) $\mathbf{1}^+$ and (b) $\mathbf{2}^+$ in THF (black line), CH_2Cl_2 (green line), and CH_3CN (red line) at room temperature and (c) $\mathbf{3}^+$ in THF.

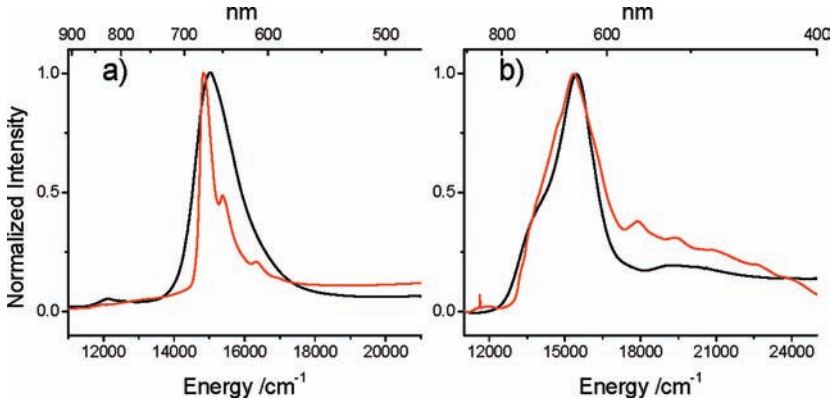

Figure 9. MLCT band for (a) $\mathbf{1}^+$ and (b) $\mathbf{2}^+$ in 2-MeTHF at 298 K (black line) and 100 K (red line).

Table 4. Energies (in cm^{-1}) of the Raman Modes for **1**−**3** Found for Excitation Resonant with the MLCT Transition

Compound	ν_1	ν_2	ν_3	ν_{MM}
1	1319	915	582	311
2	1351	933	576	367
3	1411	932	576	395

Resonance Raman of 1−3. To simulate the MLCT spectra of the complexes of interest it is necessary to identify those vibrations most strongly perturbed by this transition. It has been known for some time that one can identify these modes via resonance Raman[12,16,17] as the intensity of Raman active modes are proportional to the slope of the excited state surface. Four modes appear in the Raman spectra for **1**−**3** that are resonant with the MLCT transition. The spectra for **1** and **3** were previously reported[8] and that for **2** (taken with laser excitation at 785 nm) is reported here for the first time. The frequencies and nuclear motions associated with these modes are given in Table 4.

Simulation of the Low and Room Temperature IVCT and MLCT Bands for 1−3 and $\mathbf{1}^+$−$\mathbf{3}^+$. Using the time dependent approach of Heller,[12,13] together with the frequency of symmetric stretches obtained from Raman spectra (Table 4), the MLCT absorption spectra of **1**−**3** and $\mathbf{1}^+$−$\mathbf{3}^+$ were simulated. Figure 10 shows the simulated and experimental MLCT spectra of **1**−**3** at 298 and 100 K. Figure 11 shows the simulated and experimental MLCT spectra for $\mathbf{1}^+$−$\mathbf{3}^+$ at 298 K and 100 K. In general, the simulations are able to recreate the major features of the room temperature MLCT bands. In particular, the number and relative intensities of the vibronic features can be reliably generated. However, in all cases, the simulated spectra are not as broad as the experimental spectra (Figure 10). This "extra" broadness decreases across the series **3** > **2** > **1** and is decreased for all three complexes upon lowering the temperature. Better agreement between experimental and simulated spectra, with respect to the width of the spectra, is found for both the room and low temperature spectra of the mixed valence complexes (Figure 11). An additional problem that is evident when comparing the simulated and experimental spectra is that the spacing of the vibronic bands are slightly different. This is most noticeable in the low temperature spectra (though the agreement is remarkably good for **3** at low temperature). The slight disagreement between the spacings of the vibronic features most likely arises from the assumption in these calculations that the frequency of the Raman modes are the same in both the ground state and the excited state (see Experimental Section). We are, however, unable to determine the frequency of the Raman modes in the excited state, and so this approximation will have to suffice. However, the overall good agreement between the features of the simulated and experimental spectra seems to indicate that this assumption is not a terrible one. Discounting the general problem of vibronic spacings and broadness, we feel that for **1**−**3**, $\mathbf{1}^+$ and $\mathbf{3}^+$, the features of the spectra are extremely well captured.

There is an additional problem with the simulation of $\mathbf{2}^+$ that is worth addressing here. The large deviation

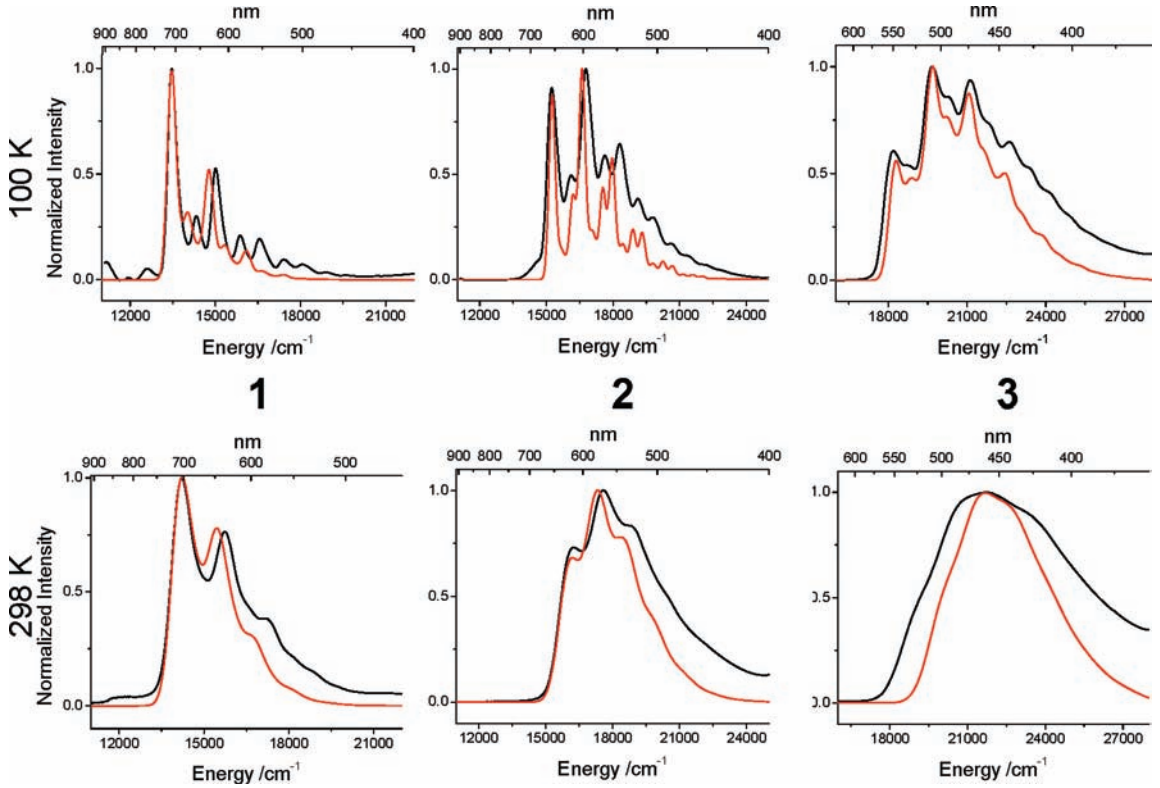

Figure 10. Experimental (black) and simulated (red) spectra of the MLCT band for **1**−**3** at 100 K (top) and 298 K (bottom). The simulations were performed using the time dependent approach to electronic spectroscopy and the energy of the Raman modes $\nu_1-\nu_3$ and ν_{MM} (Table 4).

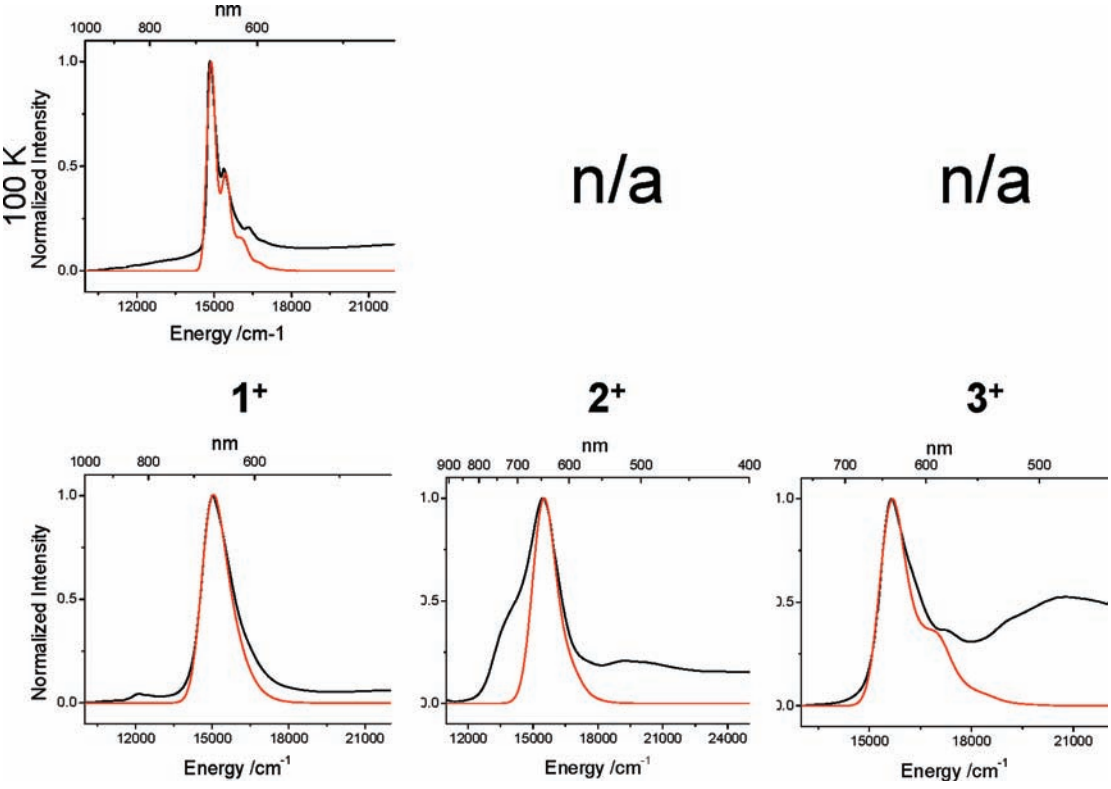

Figure 11. Experimental (black) and simulated (red) spectra of the MLCT band for $\mathbf{1}^+-\mathbf{3}^+$ at 100 K (top) and 298 K (bottom). The simulations were performed using the time dependent approach to electronic spectroscopy and the energy of the Raman modes for the neutral complexes $\nu_1-\nu_3$ and ν_{MM} (Table 4).

occurs at the low energy side of the absorption, where there is a prominent feature that is not captured by the simulation. This feature can be generated in the simulation by increasing offsets between the ground and excited

Table 5. Dimensionless Offsets (Δ) between the Ground and MLCT Excited States along the Coordinates Associated with the Raman Modes ν_1, ν_2, ν_3, and ν_{MM} for Both the Neutral and Mixed Valence States of $\mathbf{1}^+-\mathbf{3}^+$[a]

		neutral		mixed valence		percent reduction	
compound	Raman band	Δ	λ (cm^{-1})	Δ	λ (cm^{-1})	Δ	λ (cm^{-1})
1	ν_1	1.1	854	0.3	63	73	93
	ν_2	0.4	75	0.3	42	25	44
	ν_3	0.9	233	0.9	233	0	0
	ν_{MM}	0.5	49	0.5	49	0	0
2	ν_1	1.4	1324	0.4	108	71	92
	ν_2	1.0	467	0.4	75	60	84
	ν_3	0.4	47	0.4	47	0	0
	ν_{MM}	0.5	46	0.5	46	0	0
3	ν_1	1.6	1693	0.7	324	56	81
	ν_2	0.8	293	0.5	114	38	61
	ν_3	1.1	352	0.6	105	45	70
	ν_{MM}	0.5	39	0.5	39	0	0

[a] Also presented is the reorganization energy (λ) in wavenumbers associated with these dimensionless offsets.

state surfaces; however, this adds a number of vibronic features at higher energy that are not present in the experimental spectra (see the Supporting Information). As mentioned above, it is likely that this feature arises from an aggregate suspension of $\mathbf{2}^+$.[21] As such, we ignore this first feature in simulating the spectra. With these disagreements between experiment and simulation addressed, we move on to considering what parameters of interest can be extracted from the simulations, namely, the dimensionless offsets along the coordinates associated with the resonance Raman active modes. For the MLCT transitions, these are summarized in Table 5.

Let us briefly comment on some of the trends present within both the neutral and the mixed valence series. For the neutral complexes, we find that as we increase the tungsten content the dimensionless offset (1.0 for **3**, 0.82 for **2**, and 0.70 for **1**, averaged over all four modes) decreases. Using a standard approach,[16] we may extract the mode-dependent reorganization energies from these offsets. These are included in Table 5. Summing up these individual reorganization energies results in the total reorganization energy along the generalized symmetric coordinate (2377 cm^{-1} for **3**, 1884 cm^{-1} for **2**, and 1211 cm^{-1} for **1**) and gives a more intuitive picture of how dissimilar the ground and the excited state geometries are from each other. The cationic series does not have this clear trend in the dimensionless offsets for the MLCT transition. The average dimensionless offsets for $\mathbf{3}^+$, $\mathbf{2}^+$, and $\mathbf{1}^+$ are 0.50, 0.42, and 0.50, respectively, resulting in corresponding total reorganization energies along the symmetric coordinate of 582 cm^{-1}, 276 cm^{-1}, and 387 cm^{-1} for $\mathbf{3}^+$, $\mathbf{2}^+$, and $\mathbf{1}^+$, respectively.

While there may be trends *within* each series, what we are most interested in are the *changes* to the dimensionless offsets for a particular complex that occurs upon oxidation. In every case, the neutral and oxidized spectra differed from one another to a great enough extent that these offsets had to be significantly changed to obtain a reasonable simulation. Again, in every case, generation of the mixed valence ion required that those dimensionless offsets that required changing be reduced. That is, the experimental and simulated results indicate that for **1**, **2**, and **3**, oxidation results in the movement of the ground state and MLCT excited state surfaces toward each other along the symmetric coordinate. The changes in the offsets are most easily seen along those coordinates associated with high frequency Raman modes. Thus, the overall shape and features of the simulated spectra are most sensitive to changes in the offsets along the ν_1 coordinate. For the ν(MM) mode, reasonable fits are obtained assuming both a 70% reduction in the offset upon oxidation or no change in offset upon oxidation. As such, the change in offset along this coordinate is reported as zero and all of the following discussion of changes to the offsets obtained from simulation will focus on changes along the ν_1 and ν_2 coordinates. The offset of the ground and excited state surfaces along these coordinates *required* adjustment for $\mathbf{1}-\mathbf{3}$.

We have also simulated the IVCT bands for $\mathbf{1}^+-\mathbf{3}^+$ at both room and (when available) low temperature. The experimental and simulated spectra can be found in Figure 12, and the dimensionless offsets used to generate the simulated spectra are summarized in Table 6 together with the associated reorganization energies. The agreement between the experimental and simulated IVCT bands appear, in general, to be better than those for the MLCT bands. There are two trends worth commenting on concerning the dimensionless offsets associated with the IVCT transition. First, we find that the average offset (0.55 for $\mathbf{3}^+$, 0.5 for $\mathbf{2}^+$, and 0.33 for $\mathbf{1}^+$) decreases as the degree of electronic coupling increases ($\mathbf{H_{AB}}$ − as previously estimated[9] from the positions of the IVCT bands). This is reflected in the total reorganization energies along the generalized symmetric coordinate (474 cm^{-1}, 323 cm^{-1}, and 144 cm^{-1} for $\mathbf{3}^+$, $\mathbf{2}^+$, and $\mathbf{1}^+$, respectively), which show a corresponding decrease with increases in electronic coupling. Second, the average offsets are in relatively good agreement with those obtained from the MLCT band. The largest difference between the offsets for the IVCT band and the MLCT band is found to be for $\mathbf{1}^+$. In addition, we found that the dimensionless offsets along any given coordinate were not necessarily the same when comparing them for the IVCT and the MLCT transitions.

Discussion

Solvent and Temperature Dependence of the Energy of the Charge Transfer Absorptions. The temperature dependence of the electronic transitions for neutral complexes $\mathbf{1}-\mathbf{3}$ can be explained with reference to the Walsh diagram shown in Figure 13. As one transitions from D_{2d} toward D_{2h} in D_2 symmetry, the energy of the MLCT transition will decrease, giving rise to an observed red shift in this transition. The separation between the two previously degenerate MM δ orbitals can be viewed as an increase in the mixing between the two MM based orbitals that proceeds through the bridge as the molecules approximate D_{2h} symmetry. While the most stable configuration for $\mathbf{1}-\mathbf{3}$ is one of D_{2h} symmetry, the barrier to rotation in the neutral complexes was previously calculated to be fairly low, namely, between 3.0 and 4.4 kcal/mol for MM = Mo_2 and between 5.8 and 7.7 kcal/mol W_2, depending on the details of the calculation.[8] This means that the observed MLCT band at room temperature will be constructed from numerous MLCT transitions originating form a myriad of species that span a large range of

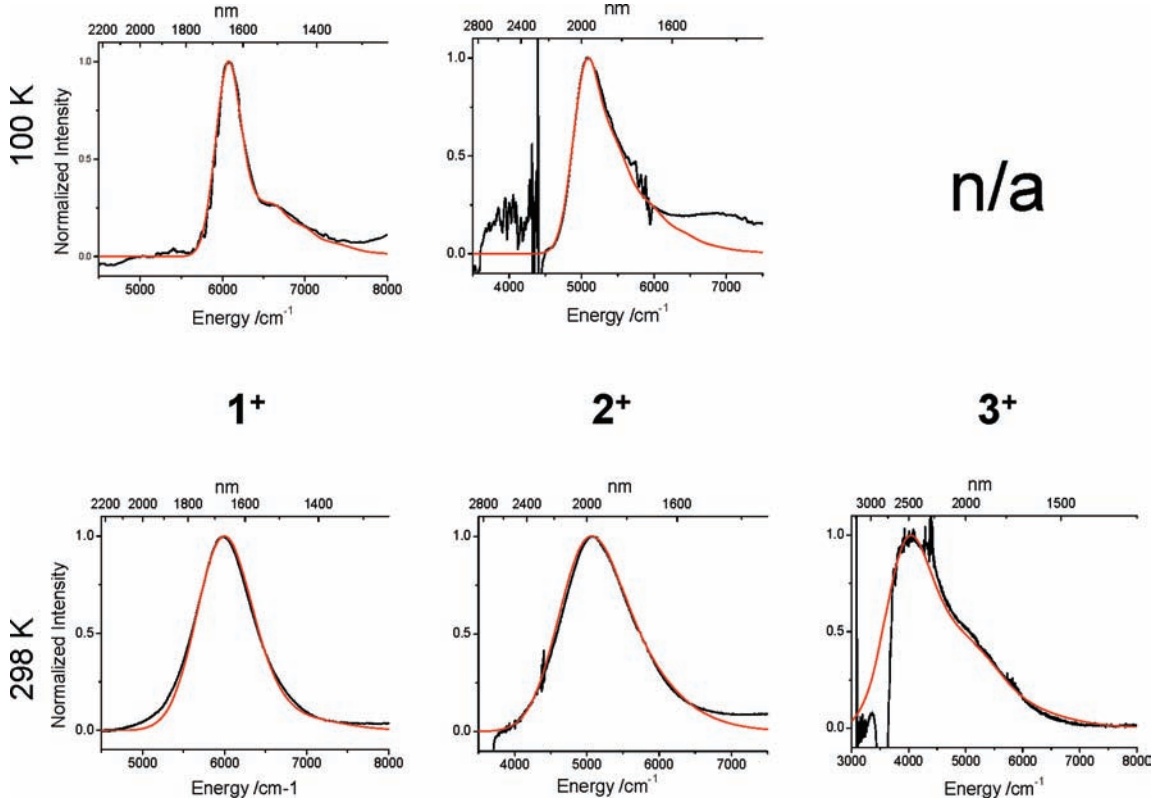

Figure 12. Experimental (black) and simulated (red) spectra of the IVCT band for $\mathbf{1}^{+}-\mathbf{3}^{+}$ at 100 K (top) and 298 K (bottom). The simulations were performed using the time dependent approach to electronic spectroscopy and the energy of the Raman modes for the neutral complexes $\nu_1-\nu_3$ and ν_{MM} (Table 4).

Table 6. Dimensionless Offsets (Δ) between the Ground and IVCT Excited State for $\mathbf{1}^{+}-\mathbf{3}^{+}$ along the Coordinates Associated with the Raman Modes ν_1, ν_2, ν_3, and ν_{MM}[a]

		mixed valence	
compound	Raman Band cm^{-1}	Δ	λ (cm^{-1})
1	ν_1	0.2	28
	ν_2	0.2	19
	ν_3	0.3	26
	ν_{MM}	0.6	71
2	ν_1	0.2	27
	ν_2	0.4	75
	ν_3	0.5	72
	ν_{MM}	0.9	149
3	ν_1	0.5	165
	ν_2	0.6	165
	ν_3	0.6	105
	ν_{MM}	0.5	39

[a] Also presented in the reorganization energy (λ) in wavenumbers associated with these offsets.

MM−MM torsion angles. The result of this is that the MLCT band will have a maximum that is shifted to higher energy than the transition for a population of pure D_{2h} symmetry (Figure 13). As the temperature in these systems is lowered, D_{2h} symmetry becomes more strongly enforced in the population and the energy of the MLCT band maximum experiences a shift to lower energy. In addition, it seems likely that the increased weighting of the population toward the D_{2h} conformer also contributes to the observed trends of decreasing overall breadth of the MLCT absorption profile and increasing resolution of the individual vibronic progressions with reduction in temperature.

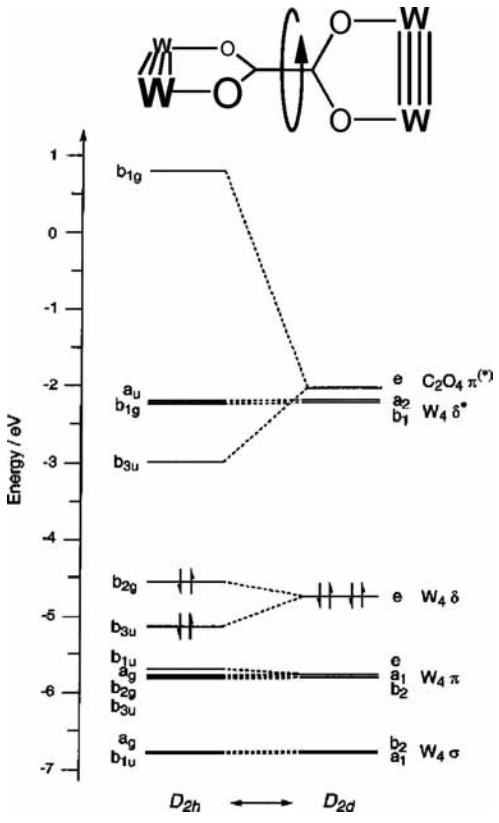

Figure 13. Walsh diagram depicting the changes in orbital energies that occur for movement between D_{2h} and D_{2d} symmetries for **1**−**3**. The depicted electronic occupation of the orbitals is for the dimers in their neutral state.

This understanding of the temperature dependence of the MLCT transition lays the groundwork for understanding both the room- and low-temperature solvent dependence for neutral **1**−**3**. At room temperature, the population of these complexes can explore a range of torsion angles, meaning that there will be a significant population of complexes that are significantly displaced from D_{2h} symmetry, resulting in weakly coupled M_2 centers. Thus, at room temperature the MLCT may proceed predominantly from one MM relative to the other, which will result in a net change in dipole moment that will be opposed by the dielectric response of the solvent, providing the origin of the solvatochromism at room temperature. As noted in the results, the degree of solvatochromism is greatly reduced upon lowering the temperature. This is a result of the fact that at low temperature D_{2h} symmetry is more strongly enforced than at room temperature. For D_{2h} symmetry the charge transferred in the MLCT transition will be more symmetrically distributed between the strongly coupled MM units and may not result in a change in net dipole moment, reducing the solvatochromism displayed by the MLCT. The fact that the solvent dependence is not fully lost may arise from the fact that there will still be a *local* change in dipole moment as the charge is symmetrically redistributed from the MM units to the bridge, or it may result from the fact that even at low temperature a significant portion of the population may remain displaced from D_{2h} symmetry. The latter explanation appears to contribute at least somewhat as can be seen from the fact that the vibronic features in DMF are less well resolved than those found in 2-MeTHF, even when both are at 100 K. DMF has a much higher freezing point than 2-MeTHF and, as a result, the population may not be as strongly weighted toward D_{2h} when the DMF freezes, locking the solute and solvent into a fixed configuration at that time. A larger spread of molecular geometries would be reflected by decreased resolution of the vibronic features, as is observed for the spectra obtained in frozen DMF. This also explains the observation that the solvent dependence observed at room temperature was reversed at low temperature. Since complexes in frozen DMF would be less strongly biased toward D_{2h} symmetry (owing to the higher freezing point of DMF) they will experience a larger dipole moment associated with the MLCT transition than for those in frozen 2-MeTHF (with a lower freezing point). This, in turn, would lead to a larger barrier for the charge transfer transition in DMF than in 2-MeTHF at 100 K. It is very important to realize that up to this point, we have been working exclusively within the orbital-picture paradigm (Figure 1c and Figure 13). As we move into discussions involving the mixed valence complexes, we will also need to consider coupling between *states*, what we will refer to as electronic coupling.

The understanding of the temperature and solvent dependence of the MLCT transition for the neutral complexes allows us to explain the solvent and temperature dependence observed for the mixed valence ions. For $\mathbf{1}^+$ and $\mathbf{2}^+$ both the solvent and the temperature dependence of the MLCT transition is greatly reduced (recall that these properties could not be examined for $\mathbf{3}^+$). Both of these phenomena can be explained by considering the effects of and requirements for electronic coupling in the mixed valence ions. All three complexes being considered had previously been assigned to class III based upon analysis of the IVCT band shape,[8−10] and the solvent independence of the IVCT band reported herein confirms that assignment. Belonging to Class III is a condition which requires a substantial degree of electronic coupling. In addition, as these complexes are symmetric, the ground electronic state is stabilized by exactly the magnitude of the electronic coupling.[22] Thus, there is a significant increase in the driving force for planarity in the mixed valence ions (associated with stabilization of the ground state). Indeed, as these complexes are class III the additional driving force (equal to the degree of coupling) is simply equal to the energy of the IVCT transition.[23] Thus, the barrier to rotation away from planarity in the mixed valence state is *increased*, relative to the neutral state, being at least 4000 cm^{-1} for $\mathbf{3}^+$, 5080 cm^{-1} for $\mathbf{2}^+$, and 5960 cm^{-1} for $\mathbf{1}^+$ (i.e., 11.4, 14.5, and 17.0 kcal/mol, respectively). Clearly D_{2h} symmetry is much more strongly enforced in the mixed valence state than in the neutral state. The result of this stronger trend toward D_{2h} symmetry is that low temperatures are no longer required to enforce this symmetry. This explains the loss, in the mixed valence state, of the temperature dependence of both the energy and the solvent dependence of the MLCT transition. We believe the observed lack of solvent and temperature dependence for the IVCT band of $\mathbf{1}^+$ and $\mathbf{2}^+$ to have the same origin as outlined above for the MLCT band. Though solvent and temperature independence of these transitions is a logical result of the orbitals that exist under D_{2h} symmetry, it is a conclusion that would also be arrived at by considering the symmetric electronic distribution of the unpaired electron expected for a class III mixed valence complex. Thus, we have two means by which to explain this loss of solvatochromism. Of course invoking the MO picture of the Walsh diagram (Figure 13), where the orbitals are delocalized over both MM units, would seem to necessitate the class III nature of the complexes and so the distinction between these two explanations may be trivial. That is, the symmetry argument given above could not be invoked if the unpaired electron was *not* delocalized.

We wish to take the time here to explicitly point out that the additional barrier to rotation found for the mixed valence systems is ascribed to the stabilization that comes from coupling between *states*. This differs from the stabilization that arises, in the MO picture, from the coupling between MM δ and bridge *orbitals*. That is to say that the stabilization gained in the mixed valence complexes is not necessarily a result of increased interaction between the MM δ orbital and the bridge LUMO. Indeed, with oxidation both the energetic alignment and spatial overlap between the MM δ orbital and the bridge LUMO should *decrease*. However, it is intuitively clear that one may expect the greatest degree of electronic coupling (electronic communication) for the D_{2h} symmetry and so the driving force between states provides a driving force for planarity. This highlights *one* of the

(22) Lear, B. J.; Kubiak, C. P. *J. Phys. Chem. B* **2007**, *111*, 6766–6771.
(23) Brunschwig, B. S.; Creutz, C.; Sutin, N. *Chem. Soc. Rev.* **2002**, *31*, 168–184.

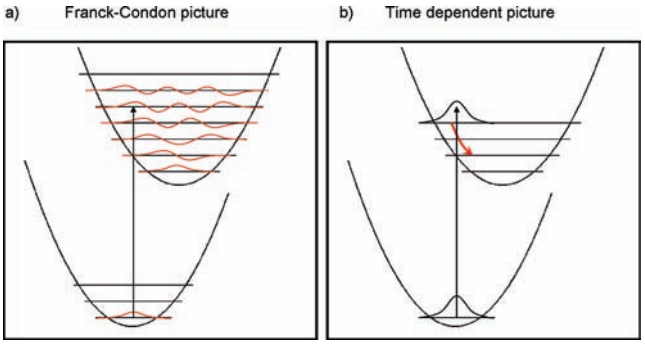

Figure 14. (a) Standard, Franck−Condon, picture associated with vibronic transitions. In this picture, the length of the vibronic transition and the intensity of each individual transition are related to the overlap of the ground and excited state wave functions. (b) A diagram that shows the origin of vibronic features from a semiclassical time-dependent viewpoint. In this picture, the overall bandwidth for an electronic absorption is related to the rate at which the dynamically evolving excited state wavepacket loses its initial overlap with the static wave function from which it originated.

differences between state and orbital based descriptions of coupling.

All in all, we see that the temperature and solvent dependencies of the charge transfer transitions in neutral and mixed valence states of **1**−**3** can be understood with reference to molecular symmetry. In particular, one needs to consider the barriers to rotation as well as the requirements for and effects of electronic coupling in these systems. With these phenomena considered, we next move onto the vibronic features present in the MLCT transition for these complexes, which promise to yield much more information concerning the PES associated with the neutral and mixed valence states.

Vibronic Features of the MLCT and IVCT Absorptions. The vibronic features (and the changes they experience with change in oxidation state, temperature, and solvent) of the MLCT and IVCT bands in **1**−**3** are of particular interest in this manuscript. Because of this, it is first worth considering the underlying origin of vibronic features. We will interpret the vibronic features of both the IVCT and the MLCT bands with reference to both the standard Franck−Condon model as well as the time dependent approach developed by Heller.[12,13] These are compared pictorially in Figure 14. The Franck−Condon approach (Figure 14a) takes into consideration the overlaps of the vibrational wave functions of the initial and final electronic states. Under the Franck−Condon treatment the degree of vibronic coupling in an electronic transition is related to both changes in equilibrium geometry (the offset along a nuclear coordinate associated with a vibrational mode of the PES involved in the transition) as well as changes to the frequency of the vibrational modes. Indeed, for any given vibrational mode, if an excitation does not result in either a change in equilibrium geometry or a change in frequency, then the electronic excitation *cannot* result in a change in vibrational quantum number. For the purposes of this paper, we will be attributing the vibronic coupling of the MLCT as resulting mostly from the offset of the PES, rather than to changes in frequency of the modes. Thus, the PES associated with complexes showing more extensive vibronic progressions can be thought to be more offset from one another than the PES associated with a transition displaying a less extensive vibronic progression. In addition, this explanation addresses the relative intensities of the vibronic features. The relative intensities are related to the degree of overlap between the initial and the final state vibrational wave functions. Thus, for very small offsets we will expect that the first vibronic feature ($\Delta\nu = 0$) will be the most intense. As displacement of the PES from each other increases we expect that higher energy transitions ($\Delta\nu > 0$) will begin to gain in intensity, eventually becoming dominant relative to $\Delta\nu = 0$. Thus, the Franck−Condon approach allows us to discuss the relative displacements of the involved PES based upon consideration of the relative intensities of the vibronic features.

In addition to the Franck−Condon picture, Heller has developed a time-dependent theory of spectroscopy,[12] in which the breadth of the absorption envelope, the vibronic spacings, and the degree to which these features are resolved are all determined by the movement of the excited state *wavepacket* upon the excited state PES following excitation (Figure 14b). A brief introduction to this is given in the Experimental Section, and more detailed explanations are available in the literature.[13,16,24] Of most utility for discussion of the absorption features of **1**−**3** will be the fact that the width of the total absorption envelope (containing all the vibronic features) is determined by the rate of the initial loss of overlap between the dynamic excited state wavepacket and the static ground state wave function from which the transition originates. That is, if the wavepacket moves quickly (slope of the PES is steep in the region of Franck−Condon overlap) the absorption band will be broad. Conversely, we may interpret a narrow absorption profile as excitation to a portion of the excited state PES that has a gentle slope (slow loss of initial overlap between wavepacket and wave function). The harmonic oscillator approximation then allows us to connect absorption band profiles to displacement of PES. The slope of the PES to which the transition proceeds will increase (giving rise to a broader absorption) as the PES are separated from one another. Thus, by invoking either the Franck−Condon model or the time dependent theory of spectroscopy the vibronic features and absorption envelope for the electronic excitations in **1**−**3** relate information concerning the relative separation of the minima of the GS and excited state PES in these complexes. On the basis of these considerations, we now address the vibronic features of the electronic transitions in **1**−**3** in their neutral and mixed valence states, framing the discussion in terms of the offsets of the ground and excited state PES.

The MLCT transition involves almost entirely the MM δ orbitals and the bridging ligand LUMO (a prediction that is supported by resonance Raman data);[8,25] we expect to be able to assign the vibronic features to either MM stretches or to modes of the bridge. The resolved vibronic spacings are much too large to be associated with the MM stretches and so they have been ascribed to bridge stretching modes. However, for each resolved progression, the spacing does not agree exactly with a

(24) Myers, A. B. *Chem. Phys.* **1994**, *180*, 215–230.
(25) Chisholm, M. H.; D'Acchioli, J. S.; Hadad, C. M.; Patmore, N. J. *Dalton Trans.* **2005**, *2005*, 1852–1857.

Raman active mode. This may result from a change in the force constants associated with these modes in the excited state or from the so-called missing mode effect.[26,19] The latter seems less likely as the largest vibronic spacing is associated with more energy than the ν_1 mode, and we find no higher energy modes than ν_1 in the Raman. This would be required to observe vibronic spacings larger than the energy associated with this mode.[19] The resulting conclusion, that the force constant for ν_1 is *larger* in the MLCT excited state, is certainly intriguing (especially considering the trends in frequency of this mode for **1**−**3**) and surely must contain insights into the nature of the excited state and this vibrational mode, but addressing this in detail is beyond the focus of this paper.

First, let us comment on the relative offsets of the PES within the series of neutral complexes **1**−**3**. As can easily be seen at low temperature (Figure 10), the relative intensity of the first vibronic feature (presumed to be the $\Delta\nu = 0$ transition) decreases as the relative content of tungsten decreases. Invoking the Franck−Condon model, we can then assume that as the tungsten content decreases the separation between the ground state and ^{1}MLCT PES increases along the symmetric coordinate. Supporting this explanation is the fact that at room temperature the width of the absorption (as measured at 1/e of the maximum intensity, see Table 2) decreases in the order **3** > **2** > **1**. Under the theory proposed by Heller, this means that the steepness of the slope of the ^{1}MLCT PES that is initially populated also decreases in the order **3** > **2** > **1**. This, in turn, indicates that the offset of the ground state and ^{1}MLCT excited state, along the symmetric coordinate, decreases as **3** > **2** > **1**. This is confirmed by the simulation of the spectra (Figure 10, Table 5). Thus, these two separate approaches both indicate that the offset along the symmetric coordinate is inversely proportional to tungsten content. This would seem to indicate that there is some property of tungsten that reduces the difference in bridge vibrational modes that arise between the ^{1}MLCT and singlet ground states.

We suggest that this property is the energy of the tungsten δ orbitals, which lie higher in energy than those of molybdenum. Thus, the δ orbital of the MM complexes, which mix with the bridge LUMO, lie closer in energy to the bridge π^* orbitals as the tungsten content increases. As the energy gap between the MM δ and bridge π^* decreases, the degree of their mixing will increase.[27] This means that as the tungsten content increases the orbital occupied by the excited state electron in the ^{1}MLCT state (Figure 1c) will gain more MM character, reducing the orbital differences between the nonbonding MM combination occupied in the ground state HOMO and the MM-bridge-MM antibonding orbital occupied by the excited state electron in the ^{1}MLCT state. Put another way, the reduction of bridge character in the ^{1}MLCT state means that the singlet ground state and ^{1}MLCT PES will be less strongly offset from one another along the symmetric coordinate, reducing vibronic coupling of the oxalate modes to the MLCT transition. This then explains the trend in vibronic features observed in the MLCT transition for neutral **1**−**3**.

The trend for the MLCT bands among $\mathbf{1}^+$−$\mathbf{3}^+$ appears to be more complicated. Unfortunately, because of the rate of redox disproportionation of $\mathbf{3}^+$, low temperature spectra of the MLCT bands for the mixed valence ion cannot be compared. Comparison of the width of the room temperature bands also is quite difficult as the MLCT band for $\mathbf{3}^+$ overlaps with that associated with **3**. Again, this owes to the rapid redox disproportionation of $\mathbf{3}^+$ to regenerate **3**. While it does appear that the MLCT band for $\mathbf{3}^+$ is quite narrow, there is the suggestion of a vibronic feature in the mixed valence state at 17360 cm^{-1}. However, this is difficult to verify. The result of this is that the trends in the shape of the MLCT band of $\mathbf{1}^+$−$\mathbf{3}^+$ cannot be accurately determined or examined in the manner we have for the neutral complexes. We can, however, comment on the very striking change to the MLCT band that occurs upon oxidation of **1**−**3** to the mixed valence state.

What accompanies oxidation of **1**−**3** to their mixed valence ions is a significant reduction in the vibronic features as well as the overall envelope for the MLCT absorption band. Employing the same reasoning as above, this indicates that the doublet ground and ^{2}MLCT excited state PES associated with the mixed valence ions are closer together along the symmetric nuclear coordinates than are the ^{1}MLCT and singlet ground state PES associated with the neutral species. This is supported by the fact that the first vibronic feature has gained in relative intensity for all three complexes upon formation of the mixed valence ion. Indeed, this feature becomes the most intense even for $\mathbf{2}^+$ and $\mathbf{3}^+$. Thus, also under the Franck−Condon interpretation the ^{2}MLCT and GS PES appear to have shifted closer together along the symmetric coordinate. Simulation of the spectra using the time-dependent approach (Figure 10 and 11, Table 5) leads to the same conclusions. Namely, the ground and excited state surface minima are *significantly* closer together in the mixed valence state, as compared to the neutral state.

One possible explanation for this behavior is that, in the mixed valence state, there is simply a greater degree of mixing between the MM units and the bridge. This would move the PES closer together along the symmetric coordinate for the same reasons as given when explaining the trend in vibronic coupling in the series of neutral molecules. However, it is difficult to see how mixing between the bridge and the MM units could be improved by oxidation of the MM units. Indeed, as pointed out earlier in the discussion, rather than increase mixing between the bridge and MM units, generation of the mixed valence state is predicted to decrease this coupling in a simple MO interpretation like the one presented in Figure 1c. An alternative explanation arises from realization of the fact that in the three state model we are not coupling orbitals, but rather *states*. That is we are not just coupling the MM δ orbital with the π^* orbital of the bridge to generate new orbitals (as is implied in Figure 1c). Instead, we are coupling the bridge based *state* (i.e., the MLCT *state*) with the MM δ based *states* (Figure 1a and b). The difference between the orbital picture and the state picture being that the mixing of states, necessarily,

(26) Tutt, L.; Tannor, D.; Heller, E. J.; Zink, J. I. *Inorg. Chem.* **1982**, *21*, 3858–3859.

(27) Changes in orbital overlap are not expected to effect the degree of coupling as the d orbitals of molybdenum and tungsten are quite similare in size.

must mix the transitions between them. Thus, it is no longer valid to discuss pure IVCT or MLCT transitions (again, as implied by Figure 1c). Instead, in the mixed valence state, each of these transitions contains character of the other.

The mixing of transitions becomes obvious when one carefully considers the effect of the coupling of states. Let us again consider the diabatic and adiabatic states shown in Figure 1a and 1b. The diabatic states represent *pure* states associated with the unpaired electron occupying either of the MM δ orbitals or the bridge LUMO. As we couple these pure diabatic states, we obtain adiabatic states that are, necessarily, mixtures of the pure states. Thus, though we obtain states that are commonly referred to as IVCT and MLCT states, it is important to realize that each of these adiabatic states contain character of each of the diabatic states. For instance, the adiabatic "MLCT" state may be predominantly constructed from the pure diabatic MLCT state, but it will, of necessity, contain contributions from the IVCT state as well as the ground state. The degree of composition of these other states, of course, depends on the magnitude of electronic coupling. Because of this, the presumably GS → MLCT transition will actually contain some GS → IVCT character (because of the composition of the ground and "MLCT" excited state surfaces). Interestingly, it must also formally contain some GS → GS transition as well, which, since it constitutes a "non-transition" will reduce the overall "change in state" associated with the transition. Upon examining the two "diabatic" or "pure" electronic transitions (IVCT and MLCT, Figure 1c) it can be seen that one of them (MLCT) formally removes electron density from the MM units and places it on the bridge while the other (IVCT) formally removes electron density from the bridge to the MM units. The mixing of these transitions (by way of the electronic coupling of the *states*) then ameliorates the CT character between the MM units and the bridge. This explains why the PES would decrease their displacement from one another along the symmetric coordinate upon the generation of the highly coupled mixed valence ions. It also highlights how using the MO picture in trying to describe mixed valence states is unintentionally misleading and may result in misinterpretation of the properties of their charge transfer transitions.

Let us next briefly consider the IVCT band of $\mathbf{1}^+$–$\mathbf{3}^+$. We find that the symmetry of these bands increases with the magnitude of electronic coupling ($\mathbf{1}^+ > \mathbf{2}^+ > \mathbf{3}^+$). Again, invoking our understanding of the mechanisms for vibronic coupling and the time dependent theory of spectroscopy as well as the three state model, we can make the statement that as coupling increases, the offsets of the PES involved in this transition are moving closer together. This would seem to have the same explanation as given for the changes in the MLCT band outlined above. Namely, coupling between states mixes the IVCT and MLCT transitions, moving the PES in the mixed valence state toward one another. However, under the standard description of the three state model, such reasoning is not obvious. We comment in detail on this next.

Concerning the Three State Model of Mixed Valency. So far we have seen that the generation of a mixed valence state has profound effects upon the electronic spectra of highly coupled mixed valence complexes. These effects have been interpreted as resulting from the effects of the coupling between electronic states that provide a great deal of "extra" driving force for planarity (resulting in the decreased temperature dependence of the MLCT in the mixed valence oxidation state) as well as a significant movement of the PES associated with the ground and excited states in the mixed valence complexes (giving rise to the decreased vibronic coupling in the MLCT transition upon generating the mixed valence ion). The effects of electronic coupling upon the MLCT band in inorganic based complexes has been an area that has been long overlooked in the literature and so it is worth considering here what can be learned from this with respect to the current models for mixed valence chemistry.

From the outset, the fact that the MLCT band is so strongly perturbed by the electronic coupling allows us to rule out the basic two state model,[1,2,23] in which the diabatic basis set consists of the two states defined by electronic occupation of one redox site or the other. There is no way for the MLCT band to be affected (especially with regard to coupling to symmetric modes[23]) as strongly as we observe without explicit consideration of a bridge based electronic state. Thus, the behavior that we observe requires a more sophisticated model than the two state theory of Marcus and Hush.

In the introduction we gave a brief description of the three state model of Ondrechen, which is the simplest model that can explicitly account for the effects of electronic coupling upon electronic transitions involving the bridge. Under this model, vibronic coupling of the electronic transitions to symmetric modes of the bridge is a result of the fact that the PES associated with the MLCT state is displaced from the ground state PES along a symmetric coordinate. Because of this, we interpreted the dramatic decrease in vibronic coupling in the "MLCT" transition as a result of the movement of these two PES toward one another. While we feel this explanation both makes intuitive sense and is supported by the data and analysis under the time-dependent theory of spectroscopy, it is *not* what is expected under the normal treatment of the three state model.

The description of the three state model, as given by Ondrechen, is usually with reference to an orbital diagram not that dissimilar to the one shown in Figure 1c. We have tried to be very explicit in the paper about the difference between an orbital based picture of coupling versus a state based one, as well as to point out the strengths and weaknesses of the former. The strength of the orbital approach is that the requirements for electronic coupling which is mediated *via* the bridge are immediately obvious. The drawback of this picture is that it suggests that the "IVCT" and "MLCT" transitions are "pure" transitions in the mixed valence state. This, in turn, leads one to believe that no matter the degree of coupling, the IVCT and MLCT bands will always retain a degree of ligand-to-metal charge transfer or metal-to-ligand charge transfer character, respectively (examine the orbital diagram in Figure 1c and note the orbital occupancy changes commensurate with each transition). Indeed, this has been quite explicitly stated as an *advantage* of this model, as it allows for the understanding that bridge based vibrations could be coupled to the

IVCT transition.[4] This explanation for involvement of the symmetric modes in the IVCT transition allowed for simulation of highly asymmetric IVCT bands in highly coupled mixed valence systems (such as the C-T ion) and remains a great success of this model. However, this same reasoning leads to the conclusion that no amount of electronic coupling would be able to eliminate the vibronic coupling of these transitions. From our analysis, we find that the PES involved in the MLCT transition are moved together along the symmetric coordinate much more than the 50% that would be expected as the upper limit given the three "diabatic" states that are used in the orbital picture (namely, the two combinations of the redox units and the bridge). Indeed, this 50% reduction would only be achievable in the limit that the non-mixed valence states were composed of these pure diabatic states, a situation that is hard to believe, given the perturbation of the oxalate stretches in even the non-mixed valence states from those of the free oxalate anion.[28] This perturbation suggests that the oxalate ligand is involved in significant mixing with the MM unit. Meanwhile, our observations suggest an approximate 70% reduction (along the ν_1 coordinate) starting from a situation that itself is not the pure diabatic states suggested by the orbital picture. This, in turn means that the degree of movement of the PES is *much* greater than the largest allowable movement under an orbital-based understanding of the three state model. Thus, there must be some other explanation for the movement of the ground and excited state PES toward one another along the symmetric coordinate. As pointed out above, when one works in the state-based paradigm, then this falls out naturally from the coupling of the states, which functions to mix the transitions between these states. Thus, we find that it is the state based picture that provides the most accurate model for our observations and we suggest that the orbital description be invoked with caution in the future.

Even more support is found for avoiding the orbital description when one considers the behavior of the IVCT bands that we have observed here. As pointed out, the great success of Ondrechen's model has been the ability to explain the highly asymmetric IVCT bands found for highly coupled mixed valence species. Again, this arises from the fact that the IVCT band, under the orbital description, *must* always retain some ligand to metal charge transfer character no matter the extent of the coupling (leading to vibronic coupling to symmetric modes of the bridge). However, based upon the observed room and low temperature IVCT for $\mathbf{1}^{+}-\mathbf{3}^{+}$ as well as the simulation of these spectra, we find that there is very little vibronic coupling in these transitions. Moreover, the vibronic coupling for this transition in these complexes is found to *decrease* with increases in coupling. This is an observation that is at odds with the orbital picture, but can easily be explained by invoking the state based description in which the transitions between states, in addition to the states themselves, become mixed as a result of the electronic coupling.

Another interesting observation reported above is that the integrated intensity of the MLCT band is far from zero, which is at odds with the behavior previously predicted in a review[23] that, under the three state model, the intensity of the MLCT band in mixed valence complexes should fall to zero as the system approached Class III. However, for our complexes, which are clearly well within Class III, we find that the integrated intensity of the MLCT bands retains a significant percentage of the oscillator strength found for the neutral complexes (Table 2). Clearly, the treatment of the three state model given in this review is not capturing the behavior of these real systems. In their review, the authors handle the coupling between the states by allowing the redox based states to only couple to the bridge based state and not with each other—and we suggest this is where the problem lies. Such a coupling scheme generates a IVCT state (in between the ground state and MLCT states) that contains no MLCT character. In other words, this manner of coupling preserves the "purity" of the MLCT and IVCT states, which was the exact problem with the orbital description. If, instead, one allows for coupling of all of the states with each other, then one realizes the mixed CT transitions and the complete loss of intensity for the ostensibly MLCT transition is no longer expected.

Thus far, we have considered the two and three-state models of mixed valence chemistry and concluded that it is the state-based picture of the three state model that most accurately captures the behavior of our systems. However, other models for mixed valence chemistry do exist, and we would like to address one more in this section, namely, the neighboring orbital model proposed by Zink and Nelsen.[29] This model continues the reasoning used to generate the three state model from the two state model and allows for participation of not only the LUMO of the bridge, but also the HOMO. For this reason, the neighboring orbital model may also be thought of as a four state model. While this model is no doubt an improvement on the three state model, it does not provide us with any new insight into the behavior we have reported for the MLCT transitions beyond that which is gained from the three state treatment. In particular, we still require coupling between all the states to mix the transitions and align the PES along the symmetric coordinate. This is because under this model the IVCT and MLCT transitions (using the orbital formalism) would still involve changes in symmetry on the bridge, and one would expect this to result in vibronic coupling of these "pure" transitions. As such, we feel that it is the three state model (using the state-based approach!) that is the simplest model that can explain and predict the behavior of the electronic transitions in mixed valence systems.

Classification of Mixed Valence Complexes. We conclude this discussion with a few brief observations concerning the implications that the interpretations of the MLCT band shape offered here have for the classification of mixed valence complexes. The distinction between Robin−Day Class I and II is traditionally defined as the difference between diabatic and adiabatic PES. That is, Class I compounds possess no coupling between their

(28) Hind, A.; Bhargava, S.; Bronswijk, W. V.; Grocott, S.; Eyer, S. *Appl. Spectrosc.* **1998**, *52*, 683–691.

(29) Nelsen, S. F.; Weaver, M. N.; Luo, Y.; Lockard, J. V.; Zink, J. I. *Chem. Phys.* **2006**, *324*, 195–201.

electronic states, while Class II compounds display significant electronic coupling, but retain electronic structures that are localized predominantly on a single redox site. The effects of this coupling are to stabilize the ground state PES, reduce the barrier to thermal electron transfer, and move the minima of the ground state PES toward one another along the reaction (asymmetric) coordinate. As Class II becomes Class III the barrier to thermal electron transfer goes to zero, and the two minima in the ground state PES merge into one another. This necessarily brings the ground and excited state PES minima in line with one another along the asymmetric (reaction) coordinate. Thus, the distinction between Class I, II, and III can be recast in terms of this PES "nesting" along the asymmetric coordinate. In such a description we speak in reference to the diabatic state and so Class I would contain those compounds for which there is no movement of the PES toward nesting (by definition). For Class II compounds the PES would have moved significantly, but incompletely, toward being nested with one another along the asymmetric coordinate and for Class III compounds the nesting would be complete. Importantly, the complete nesting along the asymmetric coordinate necessitates a single minimum in the ground state PES (and thus fulfills the traditional requirement for Class III, namely, electronic delocalization).

However, as we have seen, explicit consideration of the electronic occupation of the bridge (three state model) requires consideration of a symmetric coordinate (Figure 1a) and nesting along the asymmetric coordinate does not require simultaneous nesting along the symmetric coordinate. Thus, building upon the nesting criterion outlined above, we tentatively propose that a new classification for mixed valence compounds could exist. This would be one for which electronic coupling between states has not only nested the PES along the asymmetric coordinate (Class III) but simultaneously along the symmetric coordinate as well. This newly proposed Class, which uniquely arises from consideration of both the symmetric and asymmetric coordinates, we term Class IV. We also note that Class IV may thought of as a subclass of Class III, being that the unpaired electron will necessarily be fully delocalized (PES nested along the asymmetric, or reaction, as well as the symmetric coordinate) in such cases.

Following from the models used above (Franck−Condon and the time dependent theory of spectroscopy) we can predict the properties of the charge transfer transitions of compounds belonging to this newly proposed class. Namely, such a class would have IVCT and MLCT bands that simultaneously display both solvent independence and minimal vibronic features. We say "minimal" rather than a complete lack of features since the ground and excited states will be expected to have differing force constants, leading to some vibronic coupling. If the electronic coupling between states is strong enough, one could imagine a situation in which the ground and excited state frequencies were identical, leading to a complete loss of vibronic features. However, such strong coupling is not required to simply nest the PES. Thus, a complete lack of vibronic features is a sufficient, but not a *necessary*, condition for assignment of mixed valence complexes to Class IV. To confirm nesting along a particular coordinate, when vibronic features remain in the relevant electronic transition, one must know the excited state frequencies. In the case of $\mathbf{1}^{+}-\mathbf{3}^{+}$, this would require excited state Raman, which we, as yet, have not performed. As such, we can only assign those complexes with *no* vibronic features to Class IV at this time. Of the three complexes we have reported, $\mathbf{1}^{+}$ is the closest to fulfilling this requirement, failing only by possessing the weak vibronic progression found at low temperature in the MLCT and IVCT bands. Perhaps upon performing excited state Raman we will find that the PES are, in fact, nested along the symmetric coordinate. Certainly the mild amount of vibronic coupling present in the MLCT band for $\mathbf{1}^{+}$ does not rule out this possibility.

Conclusion

We have reported, for a series of complexes involving coupled quadruply bonded MM units, the shape, temperature dependence, and solvent dependence of the MLCT and IVCT bands associated with the neutral and mixed valence states. We have shown that the temperature and solvent dependence can both be understood with reference to the symmetry of the complexes. We have also shown that *changes* to the temperature and solvent dependence that accompany the generation of the mixed valence species can be understood by consideration of how the molecular geometry is enforced by the degree of electronic coupling.

In addition, we have considered the overall shape and vibronic features of these complexes in light of the Franck−Condon model and the time dependent theory of spectroscopy. We used these theoretical approaches to give insight into the underlying PES involved in these transitions. We found that many of the trends in these complexes can be understood by considering the magnitude and effects of electronic coupling between the electronic states within the system and the changes to the relative orientation of the PES that arise from this coupling. We have also attempted to connect these results concerning the behavior of the MLCT transition with current theories of mixed valence chemistry. We believe that the three state model for mixed valence chemistry provides an adequate framework within which to interpret these results. However, we have also been careful to distinguish between state-based and orbital-based descriptions of mixed valence complexes, pointing out the errors in understanding that can arise from mis-use of orbital-based descriptions.

On the basis of these observations, we have also suggested a new classification for mixed valence complexes, Class IV. This class and its assignment criterion (solvent independence of the MLCT and IVCT bands and minimal vibronic coupling) emerged from considering the possibility of nesting of the relevant PES along both the asymmetric (reaction) and the symmetric coordinates utilized in the three-state model. Of the complexes examined in this study, $\mathbf{1}^{+}$ lies closest to this new class, if not within it. Though it is likely that excited-state Raman will be needed to identify Class IV mixed valence complexes within the more general Class III, it is our hope that, in the future, other complexes will be found to belong to this proposed class.

In spite of the explanations forwarded to explain the changes in the MLCT bands that were observed to accompany the generation of the mixed valence state as well as the implications this has for current theory and classification,

the main thrust of this paper remains to highlight for the reader that these changes to the MLCT band do, in fact, occur. We hope that we have shown that the MLCT band is of interest in the study of inorganic mixed valence complexes and that it promises to provide much information concerning the electronic states of such complexes. In the future we hope to be able to provide a more detailed framework in which to interpret these changes with the goal that the MLCT band will become a standard probe of electronic coupling and mixed valence theory, just as is already the case for the IVCT band.

Acknowledgment. We thank the NSF for financial support of this work. We also thank Prof. Anne Kelly for kindly sending us a copy of *Ramint*. We are also indebted to both Prof. Anne Kelly and Prof. Joseph Hupp for many helpful discussions of this work.

Supporting Information Available: A figure depicting the IVCT band and its mirror image, superimposed on each other, for both $\mathbf{1}^+$ and $\mathbf{2}^+$. A figure depicted the results of fitting the MLCT band of $\mathbf{2}^+$ when the lowest energy feature is included. This material is available free of charge via the Internet at http://pubs.acs.org.